Dry Run HALO-(AC)^3 2021
Report on Weather Observations

Sebastian Becker[1], Henning Dorff[2], Benjamin Kirbus[1], Hanno Müller[1], Johannes Röttenbacher[1], Tim Sperzel[1], and Andreas Walbröl[3]

[1]Leipzig Institute for Meteorology, University of Leipzig
[2]Meteorological Institute, University of Hamburg
[3]Institute for Geophysics and Meteorology, University of Cologne

Contents

1 Introduction

In order to gain an overview of the main synoptic patterns, daily plots of sea-level pressure (Fig. 2), 850 hPa air temperature (Fig. 1) as well as total column water vapor (TCWV; Fig. 3) were created. For this purpose, the ECMWF reanalysis data set ERA5 was used. The main observed features will be discussed separately for weeks 1-3 (team Cologne) and 4-6 (team Leipzig).

2 Overview weeks 1 to 3 (08 March 2021 - 28 March 2021)

The first week of the observation period for the HALO-(AC)^3 dry run started with relatively high pressure influence and rather weak zonal winds (Fig. 2). This developed into a cold air outbreak (CAO) when a cyclone, that originated from Iceland, found its way to Svalbard and advected cold air from the central Arctic to the warm ocean in the Fram Strait on the 11th of March 2021 (Table 1). The northerly winds are supported by a strong dynamic cyclone in the Laptev Sea. Although the cyclone continued to propagate eastwards, the Laptev Sea cyclone jointly acted with an extended anticyclone over the Beaufort Sea to keep the CAO in the Fram Strait alive (Fig. 2). The cyclones around Svalbard continued to dissipate from 11th to 15th March and a high pressure influence over Greenland allowed for sustained north to north-easterly winds (Table 1). Therefore, cloud streets related to the CAO could be observed from 11th to 15th March. Cyclonic flow in high altitudes due to a trough in the 500 hPa geopotential height kept high clouds alive during this period.

Table 1: Cold air outbreak (CAO) and warm air intrusion (WAI) occurrences together with flight conditions at Longyearbyen (Svalbard) for the Polar 5 and 6 aircraft during the first three weeks of the HALO-(AC)^3 dry run in spring 2021. The strength of the red color in row CAO and WAI signifies how pronounced the respective occurrence was. Green means favourable flight conditions, yellow difficult flight conditions and red denotes a no flight day.

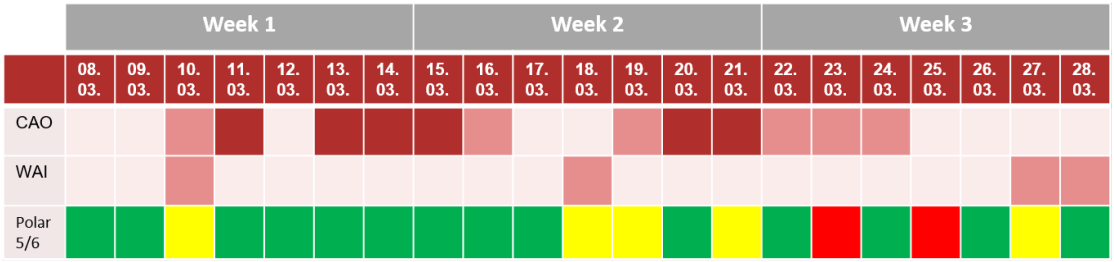

On 16 March the high pressure system propagated from Greenland towards Svalbard, disrupting the northerly winds from the previous days. As a consequence, the cloud streets lost their structure in the Fram Strait and north-easterly winds have been established to the south-east of Svalbard. The resulting CAO led to the formation of a Polar Low where cold and warmer air masses converged (see Sec. 5).

Within the next two days, the flow in the Fram Strait reversed because a cyclone propagated northwards to the east coast of Greenland while the high pressure system moved to the east of Svalbard, establishing a moderately strong southerly wind. This

resulted in a warm air intrusion of intermediate strength on the 18th March, visible from the northward extension of higher total column water vapor and warm temperatures at 850 hPa (Fig. 2-3, and Table 1). Missing support of the meridional flow in high altitudes prevented the warm and moist air to continue its journey past the latitude of Longyearbyen into the central Arctic. Within the subsequent 24 hours, the cyclone moved from Greenland to Svalbard where it remained until the 21st of March 2021. This led to intense northerly winds in the Fram Strait and another period of CAO over the open ocean to the west of Svalbard (Fig. 2-1, and Table 1). On 22 March the approach of another cyclone from Iceland disrupted the northerly winds temporarily. The two cyclones merged on the 23rd of March with the center being located to the south of Svalbard on that day. The resulting north-easterly winds in the Fram Strait missed components perpendicular to the sea ice edge and they merely recycled the air mass of the previous cyclone so that this one is not a typical CAO. On 24 March the next cyclone approached from Iceland and the merged cyclone, which split up into a rotation center west and south-east of Svalbard, propagated eastwards (Fig. 2). With this constellation, the north-easterly winds in the Fram Strait, almost parallel to the sea ice edge, persisted until the 26th of March. During the following 48 hours, the wind turned from northerly to easterly winds due to another attempt of an icelandic cyclone to transport warm and moist air past Svalbard into the central Arctic. Centered on half the distance between Iceland and Svalbard, the cyclone advected warm and moist air into the Norwegian Sea (Fig. 1-3). Again, the WAI stopped before it reached the latitude of Longyearbyen and the associated cyclone started dissipating on the 28th of March. A daily report of the first three weeks of the HALO-(**AC**)^3 dry run can be found in the HALO-(AC)^3 wiki (Overview 08th - 28th March 2021).

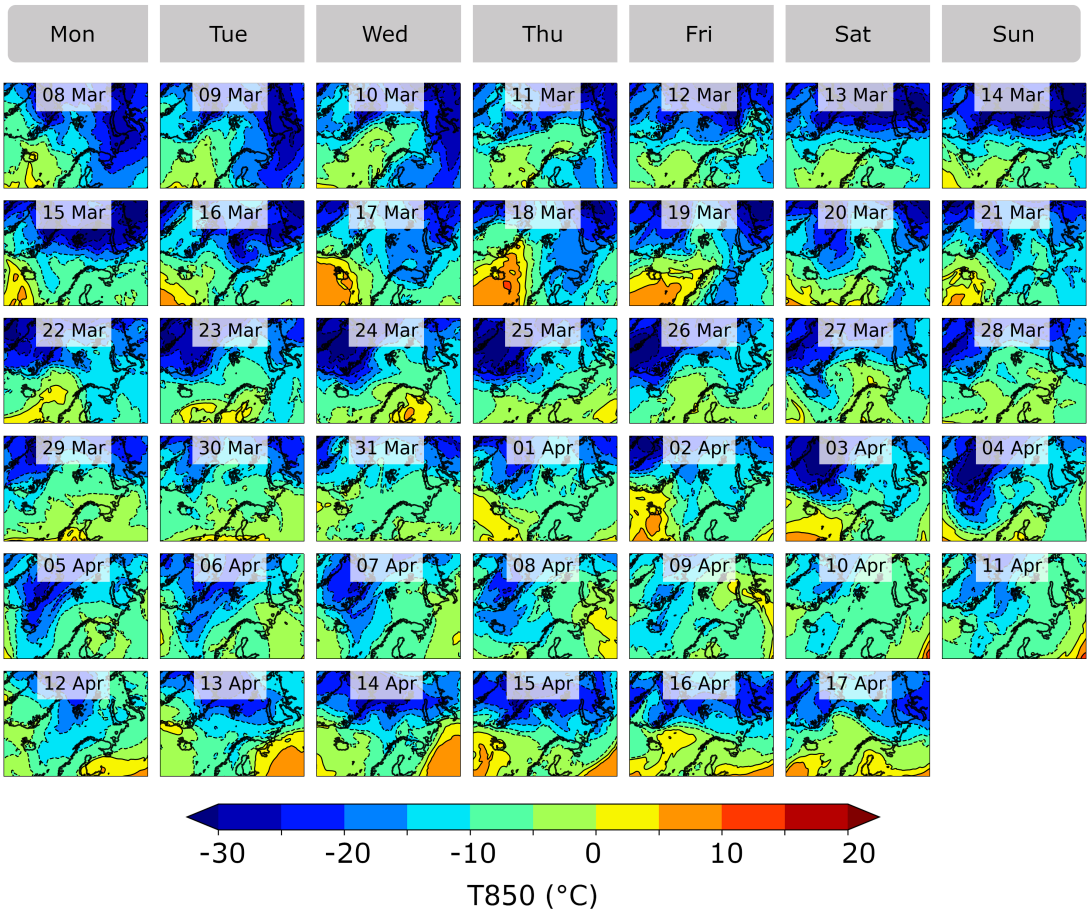

Figure 1: Daily 12 UTC air temperature at the 850 hPa pressure level (T850; from ERA5).

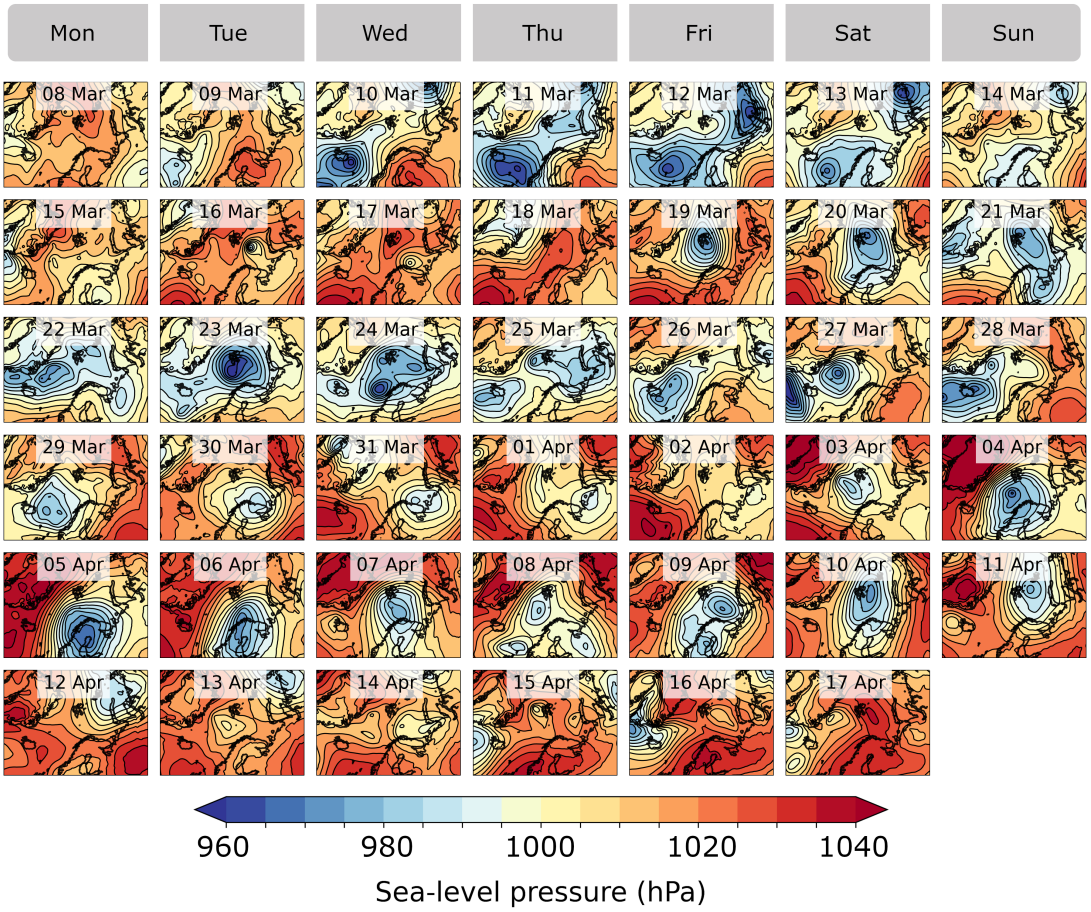

Figure 2: Temporal evolution of the daily 12 UTC sea-level pressure, as retrieved from ERA5 reanalysis.

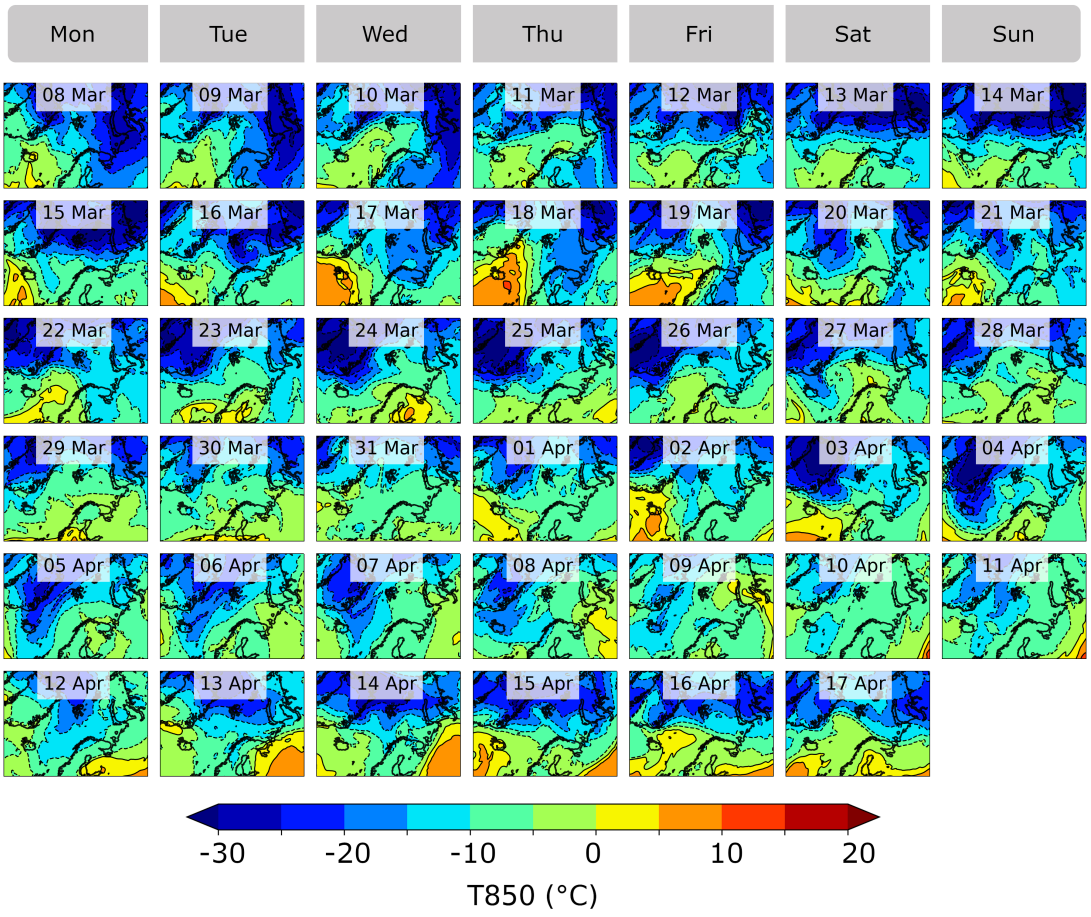

Figure 3: Daily 12 UTC total column water vapor (TCWV; from ERA5).

3 Overview weeks 4 to 6 (29 March 2021 - 18 April 2021)

As visible from Fig. 2, the first days of week 4 were characterized by a dynamic low pressure system passing from the North Atlantic eastwards towards Siberia. This low was rather weak and not directly embedded into a strong gradient, e.g. with the neighboring high over Iceland. Mostly weak winds were thus found in the vicinity of Svalbard, and neither pronounced WAI or CAO scenarios could be observed. The only exception was a slight CAO which formed around the 1st of April; here, some cloud streets flowing off the ice edge at the East of Greenland could be observed in satellite imagery.

Table 2: As Table 1 but for the second half of the HALO-(AC)^3 dry run.

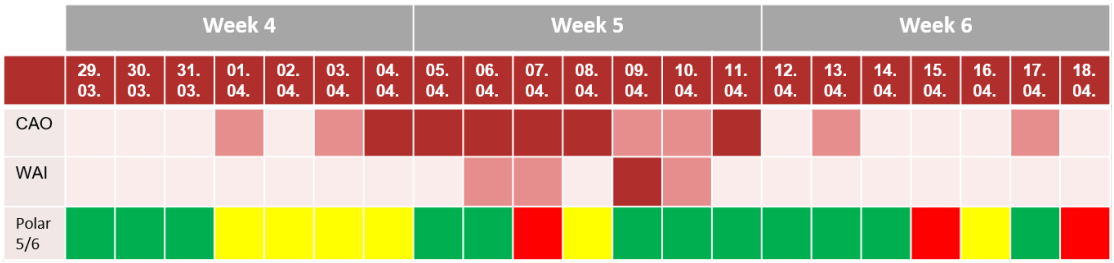

However, this rather stable synoptic situation quickly transformed. Starting on the 3rd of April, a fresh low developed south-west of Svalbard. This low deepened significantly over the subsequent days and remained lodged between the archipelago and Scandinavia for more than a week, reaching into early week 6. Combined with a constant high over Greenland, a CAO-style pressure dipole thus forced mainly northerly flows in the Fram Strait. Accordingly, consistent cold spells were visible East of Greenland in the 850 hPa air temperature (Fig. 1); also see Table 2. In parallel, increased CAO indices were found off the ice edge (Fig. 3). Interestingly, also in week 5, a slight Warm Air Intrusion (WAI) seemed to develop east of Svalbard (cf. Table 2). Synoptically, this was driven by a blocking high over Siberia and the persistent low north of Scandinavia. As a result, increased column water vapor (Fig. 3) could be observed in the Barents and Kara Seas. The combination of a southerly flow and the transport of water vapor led to a short, but marked warm spell in this region. In the subsequent days, however, the dynamic low-pressure system moved to the east. Thus, the pressure dipole was interrupted and no more WAI configuration was given. On the contrary, a small intermediate CAO formed on the 13th of April. Characteristic cloud streets covered the Whaler's Bay polynia and the ice edge almost all the way towards Novaya Zemlya. These clouds also stretched several hundreds of kilometers into the Barents Sea.

Finally, starting around 14th April, high amounts of moisture as visible from TCWV plots (Fig. 3) could be found in the North-East Atlantic sector. The synergy between a Scandinavian blocking high and a dynamic Atlantic low began driving increased amounts of water vapor towards Svalbard. However, until the end of the observation period a possible WAI scenario was suppressed by a high over Greenland's East coast; the further development of this potential WAI was not further investigated.

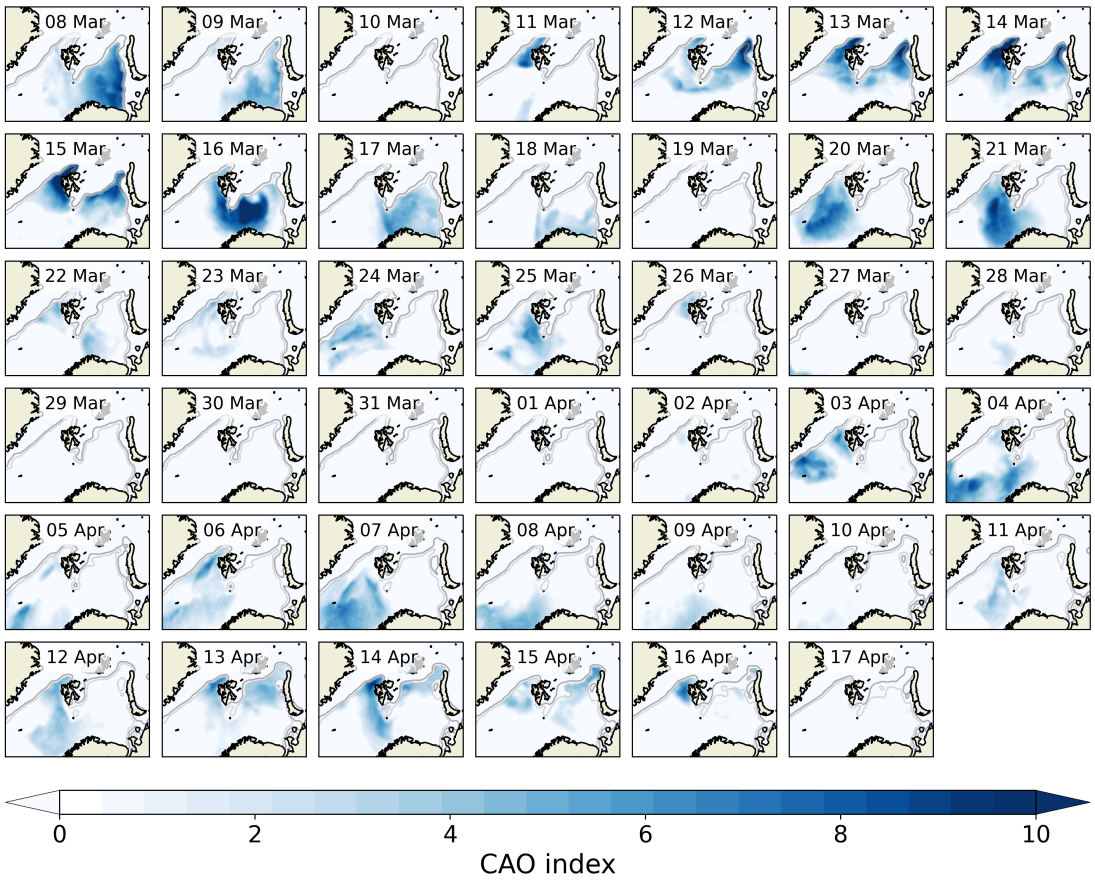

Figure 4: Temporal evolution of the daily 12 UTC Cold Air Outbreak Index (Fletcher, Mason, and Jakob 2016) close to the Svalbard archipelago. The daily sea-ice extent is marked with grey lines.

4 Marine cold air outbreak index

For all days of the dry run, the Marine Cold Air Outbreak index **M** was also calculated (Fig. 4). This index was previously shown to capture marine CAOs well. It is especially suited when using gridded climate and reanalysis data sets(Fletcher, Mason, and Jakob 2016) and shows strong correlations with low cloud boundaries and morphologies (Naud et al. 2020). Here, it is defined as:

$$\mathbf{M} = \Theta_{\mathrm{SKT}} - \Theta_{\mathrm{T800hPa}},$$

using the skin temperature (SKT) and the air temperature at the 800 hPa pressure level (T800hPa) (Fletcher, Mason, and Jakob 2016). Both variables were based on ERA5 reanalysis data (Hersbach et al. 2020). Some key messages from the graph include:

- The high number of potential CAO days becomes directly visible
- The most intense events close to Svalbard seem to have occurred in the first two weeks of the observation period
- A second pronounced CAO activity starts around the 3rd of April and again lasts about two weeks

It should be stressed that the graph only depicts the 12 UTC CAO index. Furthermore, the metric is prone to any uncertainties in the underlying ERA5 reanalysis, and **M** only focuses on static (in)stability in the lower ~200 hPa. Still, it supports the main findings about CAO occurrence as observed from satellite images and shown in Fig. 1.

5 Polar Low on 16 and 17 March 2021

On 16 and 17 March 2021 an example of a Polar Low could have been observed by HALO if the campaign had taken place this year. A Polar Low characteristically is not formed along the polar front but polewards of it. Its spatial extent usually does not exceed 1000 km and is therefore smaller than typical extratropical cyclones found in the mid-latitudes. In the following, the development of the Polar Low example will be described. A necessary ingredient for the formation of Polar Lows is a CAO, which could be observed at the ice edge to the east-south-east of Svalbard on the 16th of March 2021. The cold air that is advected over the open ocean destabilized the air mass over the warm ocean. It gathers latent and sensible heat from the water surface, causing convection in the destabilized marine boundary layer. The Polar Low can then develop in a baroclinic region where the cold air converges with warmer and more humid air. In the upper atmosphere positive vorticity advection by an approaching trough in the 500 hPa geopotential height supported the development of the Polar Low.

This Polar Low also features the characteristic cirrus shield that formed from the deep convection to the north and east of the center and the relatively cloudfree eye (Fig. 5). In the south-western part of the centre cloud streets from the CAO can be seen. The relatively warm and cloudfree core is also typical (see 850 hPa temperature in Fig. 6). Unfortunately, the Polar Low is out of reach for the Polar 5/6 aircrafts, but HALO could certainly be used to sample it. One option might be to fly multiple cross sections through the southern and northern part. On the 17th March 2021, the Polar Low already

scratches the Norwegian Coast and the positive vorticity advection has faded as it is now centered in the upper level trough. Therefore, it starts to dissipate. Only over the ocean, some convective cells can still be seen.

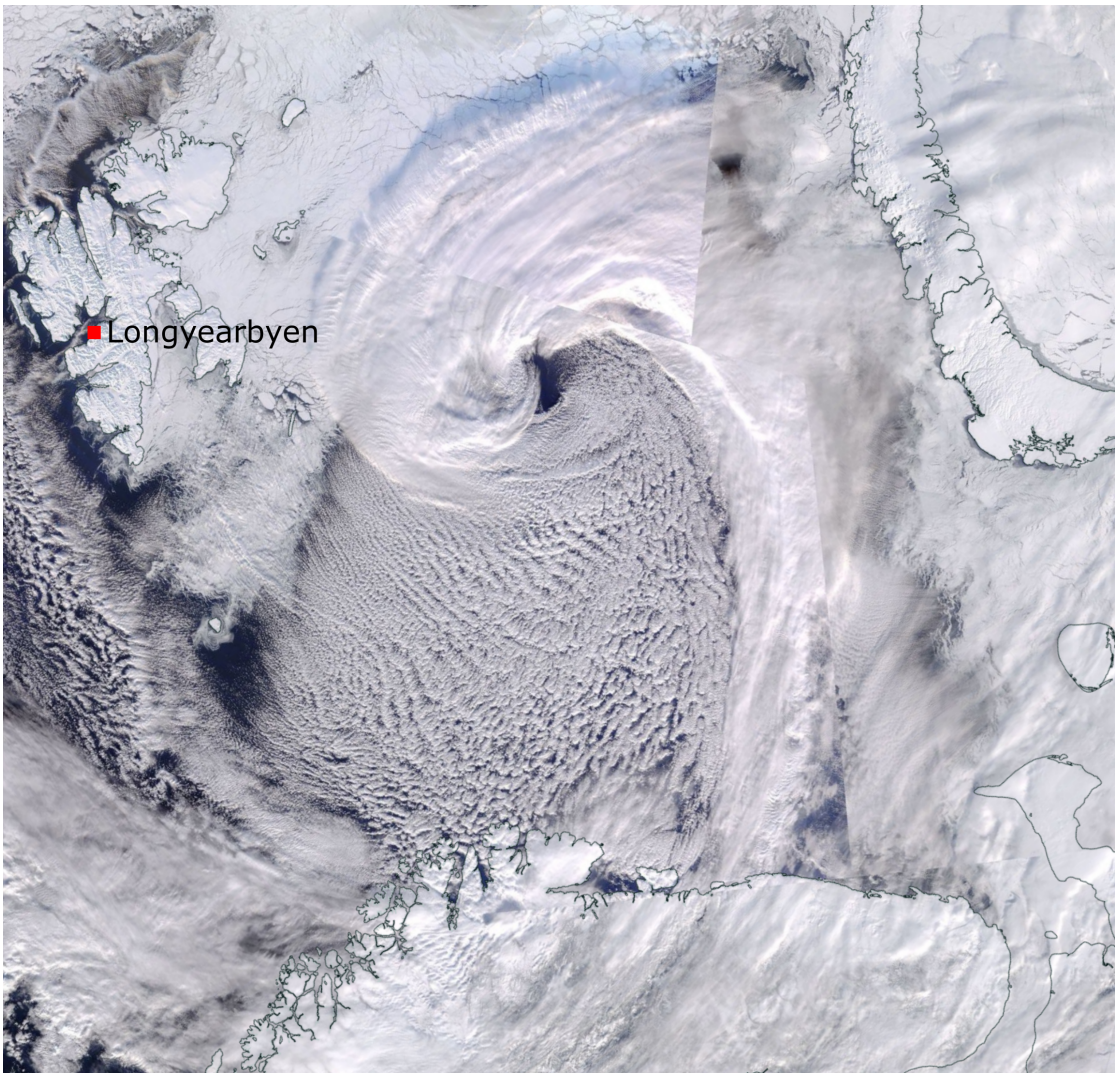

Figure 5: NOAA-20 satellite imagery from 16th of March 2021. The developing Polar Low to the east-south-east of Svalbard. Visible features are the cirrus cloud shield to the north, cloud streets from a cold air outbreak to the south and a cloudfree zone right in the center. Source: https://worldview.earthdata.nasa.gov/

6 Coexistence of cold air outbreak and warm air intrusion during week 5 (05 April 2021 - 11 April 2021

During several days of the fifth week of the observation period (mainly 7 to 9 April), both a CAO and a WAI coexisted on opposite sides of the same low-pressure system. Maps of the surface pressure, the wind field, the equivalent-potential temperature and

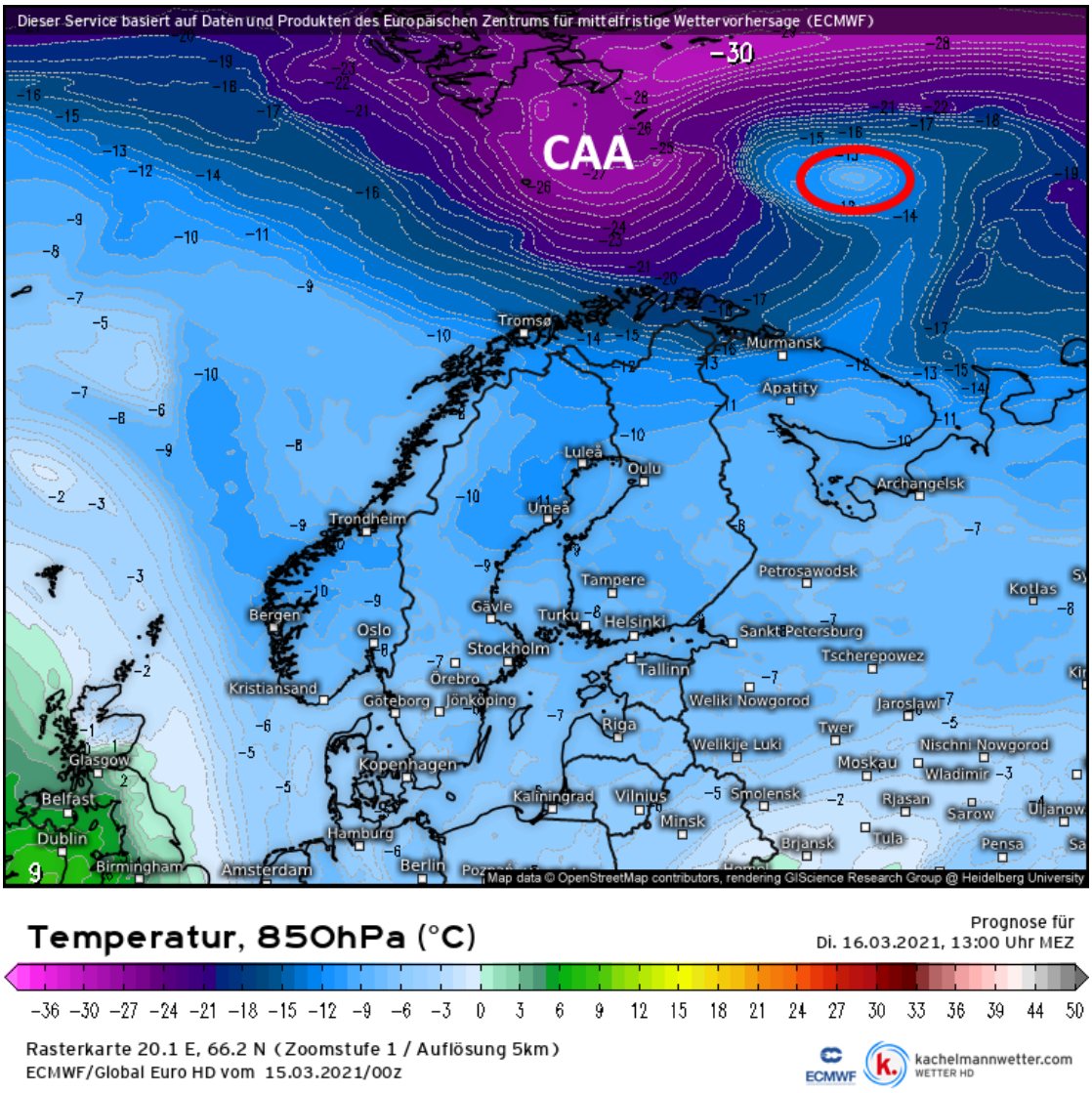

Figure 6: Temperature at the 850 hPa pressure level on the 16th of March 2021 at 12 UTC. The warm core (red circle) and cold air advection (CAA) can be seen to the south-east of Svalbard. Source: https://kachelmannwetter.com.

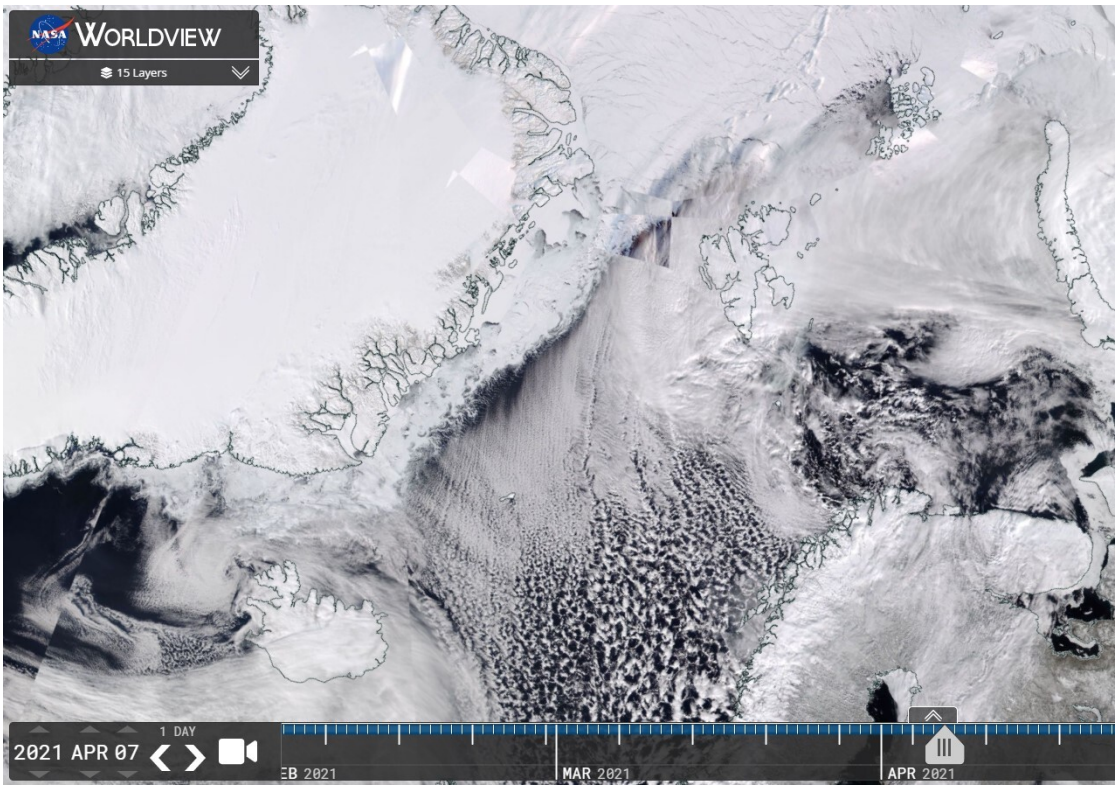

Figure 7: NOAA-20 satellite imagery from 7th of April 2021. Pronounced cloud streets are visible, flowing off the sea-ice edge east of Greenland towards Northern Europe. Source: https://worldview.earthdata.nasa.gov/

geopotential in 850 hPa, and the precipitable water are displayed in Fig. 8 for these three days. The low had already developed at the end of the fourth week (3rd April) between Scandinavia and Svalbard. Together with a high located over Greenland it caused a CAO with strong northerly winds in the Fram Strait. After an intensification lasting for two days, the low-pressure system started to weaken. The high slightly strengthened and weakened several times. However, the pressure gradient remained large being responsible for the persistent CAO. The satellite image from the 7th April shown in Fig. 7 reveals the cloud street structure over the open ocean of the Fram Strait, which is typical for CAO off-ice flows.

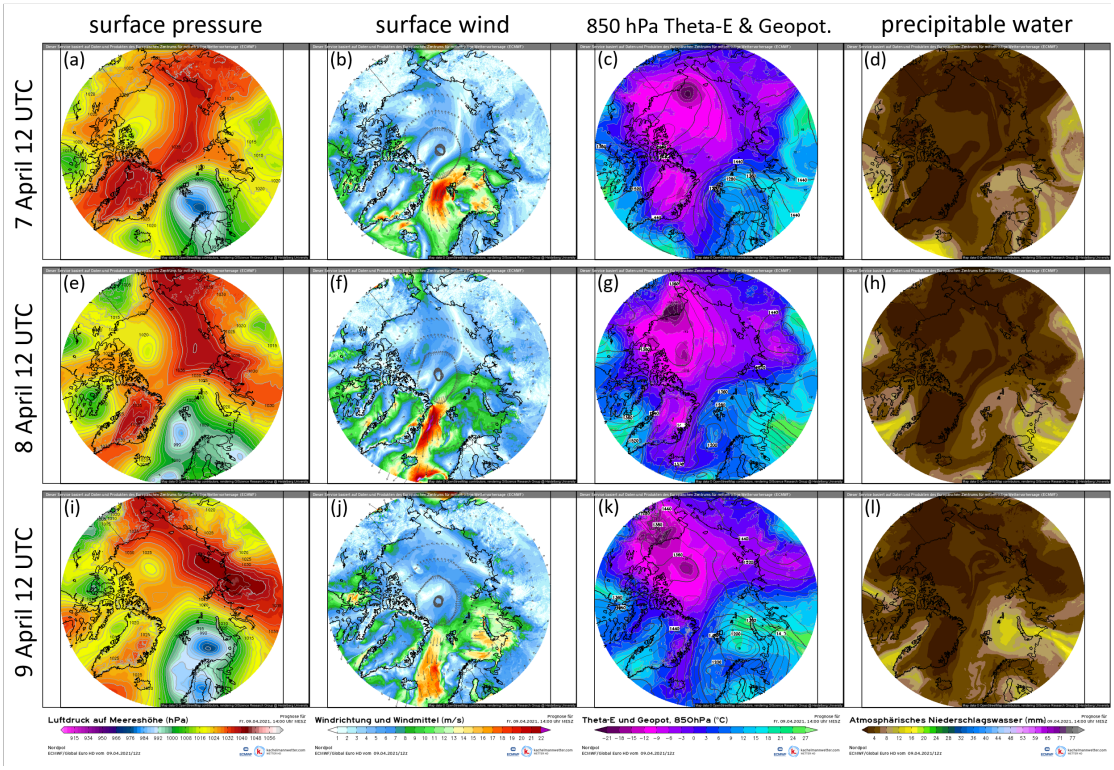

Figure 8: Maps of the surface pressure (a, e, i), the wind speed and flow direction (b, f, j), the equivalent-potential temperature and the geopotential in 850 hPa (c, g, k) and the precipitable water (d, h, l) for the 7 April (a-d), the 8 April (e-h) and the 9 April (i-l). The maps are adapted from https://kachelmannwetter.com and are based on the weather prediction of ECMWF.

From the 6th of April onwards, the high started to extend and united with a second high originating from eastern Siberia. Together they formed a large high-pressure zone over the Central Arctic containing a ridge located over western Siberia (see Fig. 8a). While the northerly flow was still strong on the 7th of April (Fig. 8b) and, thus, the COA was still active in the Fram Strait. This pressure field drove a southerly flow at the east side of the low (Fig. 8b). The equivalent-potential temperature in a pressure altitude of 850 hPa (Fig. 8c) was enhanced in this region, indicating warmer and moister air masses advected from western Siberia into the Barents and Kara Seas. In the following days, the high-pressure zone split into two cores over Greenland and the Laptev Sea. While the first

one was stationary and weakened, the second one intensified and moved south-eastward (Figs. 8e and 8i). Although the southerly flow weakened on the 8th of April (Fig. 8f) because of the weakened pressure gradient, the air mass warmed and moistened further (Figs. 8g and 8h). Finally, on the 9th of April the moist air reached the Barents Sea (Figs. 8k and 8l) with increased wind speed (pressure gradient), while the CAO in the Fram Strait weakened (Fig. 8j). Although the WAI was short and weak compared to the persistent CAO during this week, such constellations could be interesting. As shown in the pressure fields (Figs. 8a, 8e, 8i) and also indicated by the wind field (especially Fig 8b), the southerly flow around the low at its east side and the northerly flow at its west side seem to be connected. This indicates that air masses advected by WAIs cool down in the Central Arctic and are then redirected southwards in a CAO. The transformation of such air masses between the WAI and the CAO could be interesting to study by using the HALO aircraft during the upcoming HALO-(AC)^3 campaign.

7 Climatological Deviation

In order to further elaborate on the atmospheric conditions during the dry run, the following section considers its deviation from the long-term mean for various quantities. The results allow us to better assess the meteorological representativeness of the dry run for subsequent years, especially for the period of the actual HALO-(AC)^3 flight campaign in 2022. In order to cover the inter-annual variability, we use a 30-year mean reference period. This is chosen for the period of 1991-2020 to approximate as closely as possible the current climate state over the North Atlantic and Arctic Ocean, which is changing rapidly due to Arctic amplification (Pithan and Mauritsen 2014). For this purpose, we consider ERA-5 reanalysis data for the extended North Atlantic region (longitude: -70 to 80°E, latitude: 50 to 90°N) by including the dry run period (March 8 - April 17) for all years from 1991 to 2021.

7.1 Temperature 850 hPa

We focus on the temperature deviation at the 850 hPa pressure level to detect warming/cooling of air masses relative to the reference period. Temperature deviations at this level nicely represent arctic air mass deviations that may be advected by meridional transports and even can exhibit surface interactions. In this context, Fig. 9 illustrates the geospatial distribution of the 850 hPa temperature deviations for the dry run period against the 30-year reference period (1991-2020).

Overall, the HALO-(AC)^3 dry run period was not characterized by extreme temperature deviations as T850hPa-anomalies remained below +/- 4 K for our region of interest. However, two specific regions are worth investigating. These are, first, the open North Atlantic indicating a climatologically warm dry run period (up to +2 K) extending into the Barent Sea and the Greenland Sea to the sea ice edge and second, the eastern part of Greenland with a weak cold-air tongue extending toward Iceland, where six-week averaged temperature deviations reveal values around -1 to -2 K compared to 1991-2020. Cold air masses were preserved over the Greenland east coast. Even averaged over the six weeks, the dipole structure (see Sec. 3) leading to CAOs oriented along the sea ice boundary western of the Fram Strait towards Iceland resulted in stronger negative T850hPa deviations in the long-term comparison. Along Greenland the sea-ice edge

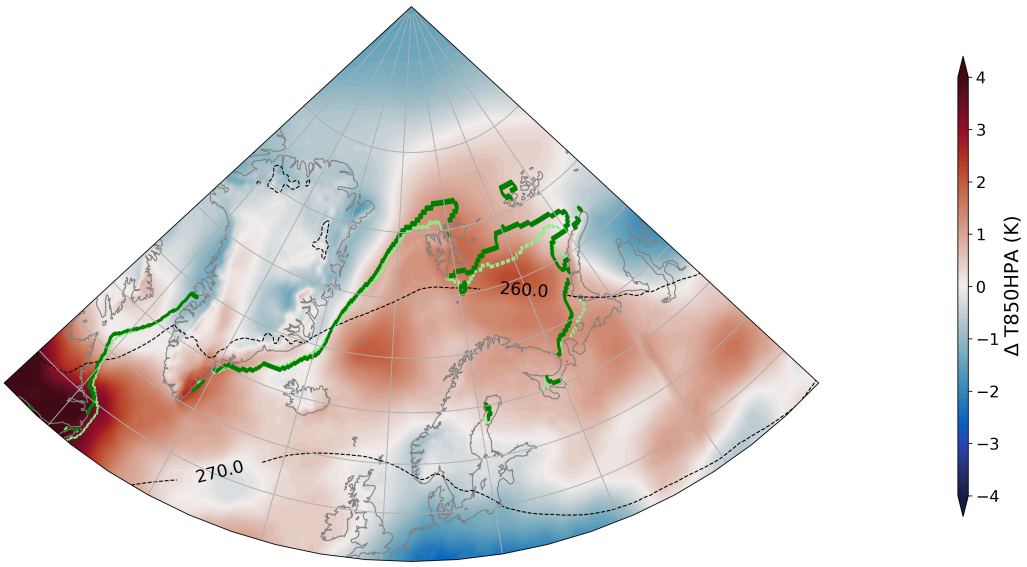

Figure 9: Deviation of 850 hPa temperature in 2021 to long-term average (1991-2020) based on the dry run period (March 8 - April 17). While coloured contours show the deviations to the long-term mean, black dashed lines indicate absolute values of 850 hPa temperature average over the long-term period in Kelvin. Statistics are based on ERA-5 reanalysis. Greenish lines depict ERA-5 average sea ice edges (light green for long-term average, dark green for dry run period 2021).

during the dry run does not indicate strong anomalies compared to 1991-2020. In turn, the warm marine regions seem counterintuitive when we consider the increased frequency of CAO during the dry run observation period. However, as illustrated in Fig. 1, the CAOs over the Barent Sea occurred primarily at the beginning (through March 17) or showed less cooling impacts towards the end of the observation period (about April 12-16). While northward warm air advection from the North Atlantic had a strikingly warm footprint that resulted in positive temperature deviations consistent with northward sea ice edge anomalies around Svalbard (Fig. 10), dominantly intermittent CAOs did reduce anomalies in some regions (e.g south of Svalbard), but without overcompensating for the overly warm environment. Nevertheless, warm air intrusions were not that intense and far-reaching into the Arctic during the dry run which manifests in negative temperature anomalies around the Pole (between -1 to $-2\,\mathrm{K}$).

7.2 Water vapor

Meridional air mass transport in the Arctic, in particular warm air intrusions, are strongly associated with transport of moisture. While less than 30% of water vapor transport events into the Arctic are related to warm air intrusions (Woods, Caballero, and Svensson 2013), they are responsible for the majority of total water vapor mass transport (moisture flux) into the Arctic in winter (Johansson et al. 2017) and throughout the year (Nash et al. 2018). Since the dry run period was characterised by less intense warm air intrusions, we here examine moisture anomalies in terms of Integrated Water vapor (IWV) in Fig. 10 and its transport, defined as Integrated Water vapor Transport IVT (Fig. 11). Starting with IWV (Fig. 10), the regions of positive and negative IWV anomalies (compared to 1991-2020) are located around those of the respective temperature anomalies. Since IWV is an absolute moisture quantity, this results from the fact that northward currents advect air masses having enhanced capacity of holding moisture that rises with temperature. Accordingly, dominating cold air masses along the sea-ice edge east of Greenland contained considerably less moisture than on long-term average. Negative six-week anomalies there range to $-1\,\mathrm{kg\,m^{-2}}$ compared to typical IWV values of around $5\,\mathrm{kg\,m^{-2}}$.

Anomalies of the moisture transport, quantified by the IVT, show a slightly different pattern. Positive anomalies of IVT over the North Atlantic pathway are in accordance with the anomalies T850hPa and IWV. Strikingly high deviations are seen upstream and downstream of Denmark Strait but do not extend farther than 70° N. Around Svalbard, the IVT anomalies feature a dipole structure with negative anomalies south of Svalbard and positive, but rather low anomalies north of Svalbard. This structure is partly a consequence of the cyclogenesis over Svalbard that led to a persisting low-pressure system in mid-March that prevented long-range meridional transport of moisture from southern sources. Subsequently, warm, relatively moist advection in the second week of April originating from the western end of Siberia (also visible in Fig. 2-3), that reached north of Svalbard, had a dominant impact that overcompensated for the precedent opposing patterns. Since these paths of warm moisture transport are typically more pronounced in May and June, their early occurrence in 2021 is worth further investigation. The lack of notable warm air intrusions over the Arctic Ocean resulted in negative deviations in IVT, similar to T850hPa and IWV.

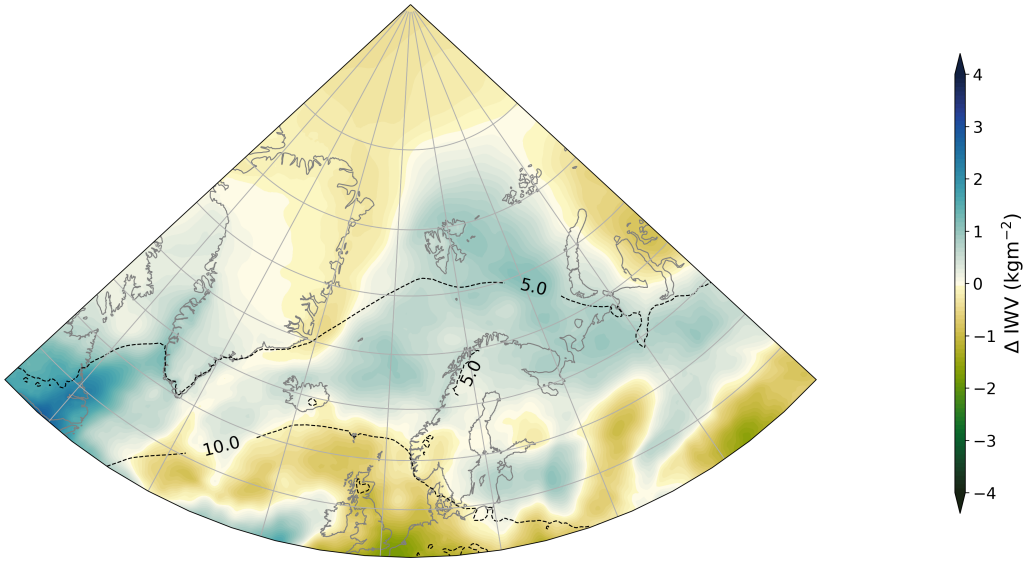

Figure 10: Analogue to Fig. 9, but for integrated water vapor (IWV) in $\mathrm{kg\,m^{-2}}$ from ERA-5.

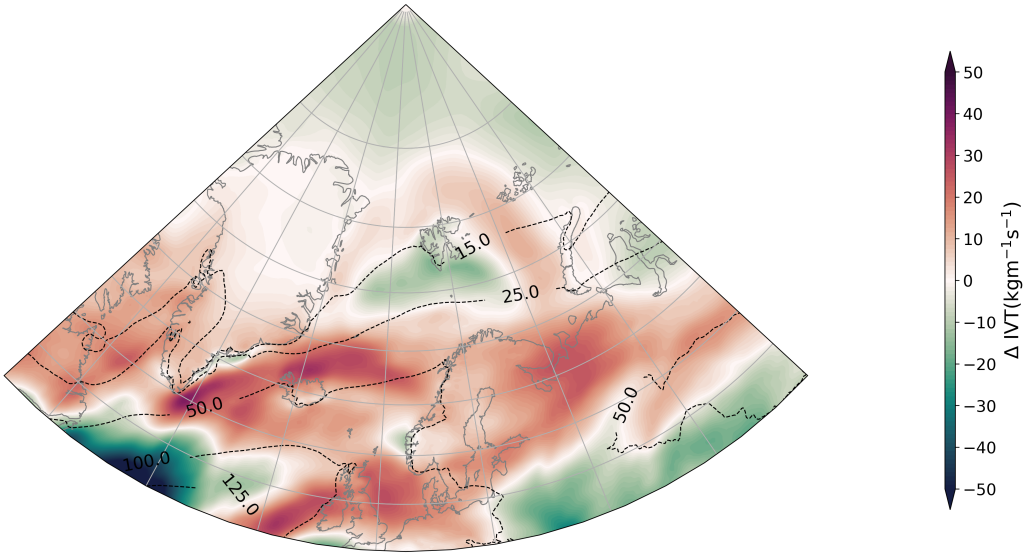

Figure 11: Analogue to Fig. 10, but for integrated water vapor transport (IVT) in $\mathrm{kg\,m^{-1}\,s^{-1}}$ from ERA-5.

8 Flight hours budget

Having looked at the general weather situation during the dry run and some days in more detail, the question remains as to how many flights we could have performed during these six weeks in 2021, the year before the HALO-(AC)^3 campaign. To get a feeling for this we checked the weather conditions for start and landing on days which show interesting meteorological features such as cold air outbreaks or warm air intrusions. As a prerequisite it is worth mentioning how many flight hours are available to us for each aircraft. We have 120 flight hours plus a number of hours sponsored by the Max-Planck-Institute Hamburg for HALO including the ferry flight to Kiruna and back to Oberpfaffenhofen. This should be enough for about 13 or 14 flights. For Polar 5 and 6 we have 80 flight hours each including the ferry flights from Bremen to Svalbard and back, leaving us with about 65 hours and roughly 12 or 13 flights. Regarding the flight conditions, for the HALO aircraft conditions at Kiruna were almost always favourable for a flight. Thus, only days on which all three aircraft would have been able to fly are counted. Polar 5 and 6 have roughly enough fuel for a five hour flight. HALO on the other hand can fly between eight and ten hours. The ferry flight from Kiruna to Svalbard takes about an hour, leaving at least six hours of flight time for collocated measurements. We consider five hours for Polar 5 and Polar 6 and eight hours for HALO as normal flight times. An overview of possible flight days can be found in Table 1 and 2. During the six weeks of the dry run favourable flight conditions for Polar 5 and 6 occurred at 23 days, from which 15 days coincided with meteorological situations of interest. Of these 15 days, eleven days fall on days with pure CAOs, three days on combinations of CAOs and WAIs and one day on a pure WAI. The rarer WAIs occurred on eight days (mostly not pronounced) within the six weeks, but for half of these eight days the flight conditions were not suitable for Polar 5 and 6. The mentioned 15 days with interesting meteorological situations exceeds the number of possible flights of 12/13 for the Polar aircraft and 13/14 for HALO. Even though the situation in 2022 may of course be different, we conclude to concentrate with the measurement flights on the one hand on the strong CAOs. Days with only weak CAOs should be used to save flight hours. On the other hand we recommend to use WAI days with conditions not suitable for Polar 5 and 6 for flights with the HALO aircraft only.

9 Summary

The HALO-(AC)^3 dry run weather observations took place from Monday, March 8, until Sunday, April 18. The observations made in the first three weeks were mainly dominated by CAO as well as some weaker WAI. From the 10th of March until the 16th of March a first phase of a consistent CAO was observed being mainly under the influence of a high-pressure system over Greenland and dissipated low-pressure systems around Svalbard. A similar situation with strong CAOs and concomitant intense northerly winds in the Fram Strait was observed at the end of week 2. The second half of the observational period was dominated by an intense and persistent CAO situation from the 3rd of April until the 11th of April. This period was characterized by a persistent high-pressure system over Greenland with a persistent low-pressure system south of Svalbard. With its strong pressure gradient, the CAO situation showed strong northerly winds in the Fram Strait. Additionally, on the 9th of April, a high-pressure system over

Siberia developed and supported a WAI at the Barents and the Kara Sea. During the observational period of six weeks, twelve days were characterized as stronger CAO and 13 days as lower CAO situations. Furthermore, one day with a strong and seven days with a weaker WAI were observed. Partly both, WAI and CAO, were observed on the same day, which might be an interesting constellation for the campaign itself. From a financial point of view, the available funding covers 13 to 14 flights of HALO and twelve to 13 flights of Polar 5 and 6, both including the ferry flights. Since HALO was during the observational period always able to start, the number of possible flight days was limited to the circumstances of Polar 5 and 6 at Svalbard Airport. By observing the conditions at Svalbard airport, 15 days were selected with good weather conditions for start and landing, as well as meteorological situations being of interest. Those 15 possible days within the observational period exceed the number of possible and funded flights for the aircrafts slightly.

References

Fletcher, Jennifer, Shannon Mason, and Christian Jakob. 2016. "The Climatology, Meteorology, and Boundary Layer Structure of Marine Cold Air Outbreaks in Both Hemispheres." *J. Climate* 29 (6): 1999–2014. https://doi.org/10.1175/jcli-d-15-0268.1.

Hersbach, Hans, Bill Bell, Paul Berrisford, Shoji Hirahara, András Horányi, Joaqun Muñoz-Sabater, Julien Nicolas, et al. 2020. "The ERA5 Global Reanalysis." *Quart. J. Roy. Meteor. Soc.* 146 (730): 1999–2049. https://doi.org/10.1002/qj.3803.

Johansson, Erik, Abhay Devasthale, Michael Tjernström, Annica M. L. Ekman, and Tristan LEcuyer. 2017. "Response of the Lower Troposphere to Moisture Intrusions into the Arctic." *Geophys. Res. Lett.* 44 (5): 2527–36. https://doi.org/10.1002/2017gl072687.

Nash, Deanna, Duane Waliser, Bin Guan, Hengchun Ye, and F. Martin Ralph. 2018. "The Role of Atmospheric Rivers in Extratropical and Polar Hydroclimate." *J. Geophys. Res. Atmos.* 123 (13): 6804–21. https://doi.org/10.1029/2017jd028130.

Naud, Catherine M., James F. Booth, Katia Lamer, Roger Marchand, Alain Protat, and Greg M. McFarquhar. 2020. "On the Relationship Between the Marine Cold Air Outbreak M Parameter and Low-Level Cloud Heights in the Midlatitudes." *J. Geophys. Res. Atmos.* 125 (13). https://doi.org/10.1029/2020jd032465.

Pithan, Felix, and Thorsten Mauritsen. 2014. "Arctic Amplification Dominated by Temperature Feedbacks in Contemporary Climate Models." *Nat. Geosci.* 7 (3): 181–84. https://doi.org/10.1038/ngeo2071.

Woods, Cian, Rodrigo Caballero, and Gunilla Svensson. 2013. "Large-Scale Circulation Associated with Moisture Intrusions into the Arctic During Winter." *Geophys. Res. Lett.* 40 (17): 4717–21. https://doi.org/10.1002/grl.50912.